Optical homodyne RZ-QPSK transmission through wind tunnel at 3.8 and 1.55 μm via wavelength conversion

Pak S. Cho*, Geof Harston, Kai-Daniel F. Büchter[a], David Soreide[b], Jonathan M. Saint Clair[c], Wolfgang Sohler[a], Yaakov Achiam, and Isaac Shpantzer
CeLight, Inc., 12200 Tech Road, Silver Spring, MD 20904
[a]Angewandte Physik, Universität Paderborn, Warburger Str. 100, 33090 Paderborn, Germany
[b]Optimal Aerospace, 6274 20th NE, Seattle, WA 98115
[c]Boeing Co., PO box 3999 m/s 3W-54, Seattle, WA 98124

ABSTRACT

Atmospheric absorption, scattering, and turbulence are impairments in practical high-speed free-space laser communications. These atmospheric effects can be mitigated by choosing the proper transmission wavelength. It is well known that the MWIR (~3.8 μm) has many low-absorption spectral lines suitable for low-loss propagation. Also, MWIR can be more robust to turbulence in the weak-turbulence regime. Since high-speed laser transceivers are not available in the MWIR, a 3.8-μm signal can be generated and detected using a 1.55-μm telecom transceiver via wavelength conversion. Free-space transmission of optical homodyne RZ-QPSK through a turbulent channel at 3.8 μm has been investigated. A pair of Ti:PPLN-based nonlinear wavelength converters were used to down- and up-convert from 1.55 to 3.8 and back to 1.55 μm at the transmitter and at the homodyne receiver, respectively. The converted RZ-QPSK signal was transmitted through a tabletop wind tunnel that produces a weak turbulent path. Comparison of 1.55 and 3.8 μm transmission through the wind tunnel shows that under weak-turbulence 3.8 μm transmission is more robust than 1.55 μm. Under the same turbulence condition, the scintillation index measured at 3.8 μm is consistently lower than that at 1.55 μm. Extrapolated scintillation indexes for 3.8 and 1.55 μm using the Rytov variance ($\sim \lambda^{-7/6}$) and independent measurement at 632.8 nm are consistent with the RZ-QPSK scintillation data for 3.8 and 1.55 μm. Under the most severe turbulence condition, the average bit-error-rate of 3.8-μm transmission is better than that of 1.55-μm giving an estimated receiver sensitivity improvement of at least 6 dB.

Keywords: free-space laser communications, coherent communications, turbulence mitigation, quadrature phase-shift-keying, homodyne detection, Ti:PPLN integrated nonlinear wavelength conversion, MWIR atmospheric transmission.

1. INTRODUCTION

Atmospheric extinction (absorption and scattering) and turbulence are impairments in practical high-speed free-space laser communications systems. Inhomogeneities in the temperature and pressure of the turbulent atmosphere lead to variations of the refractive index along the transmission path. Optical wavefront distortion as a result of the aero-optical effect leads to optical intensity fluctuation or scintillation. Absorption, on the other hand, diminishes the optical power available at the receiver but does not produce significant scintillation. Both of these impairments can be mitigated by choosing the proper optical wavelength for transmission. It is well known that in the MWIR region (~3.8 μm) there are many low-absorption spectral lines in several sub-bands that are suitable for low-loss propagation[1]. Furthermore, extraneous thermal and solar background emissions are relatively low in this spectral band. Fig. 1 shows transmittance data in the 1.5-1.6 μm and the 3-4 μm bands over a 100 km path. In addition to lower absorption, MWIR can be more robust to turbulence than shorter wavelengths in the weak turbulence regime[2]; this is supported in recently reported transmission experiments[3]. Since a practical high-speed (GHz) laser transceiver is not available at 3.8 μm, a 1.55 μm telecom type transceiver can be used in conjunction with wavelength down- and up-conversion, namely 1.55 to 3.8 μm and back to 1.55 μm, to produce an equivalent transceiver at MWIR.

* pscho@celight.com; phone 1 301 625-7000; fax 1 301 625-7001; celight.com

Atmospheric Propagation VI, edited by Linda M. Wasiczko Thomas, G. Charmaine Gilbreath,
Proc. of SPIE Vol. 7324, 73240A · © 2009 SPIE · CCC code: 0277-786X/09/$18 · doi: 10.1117/12.810498

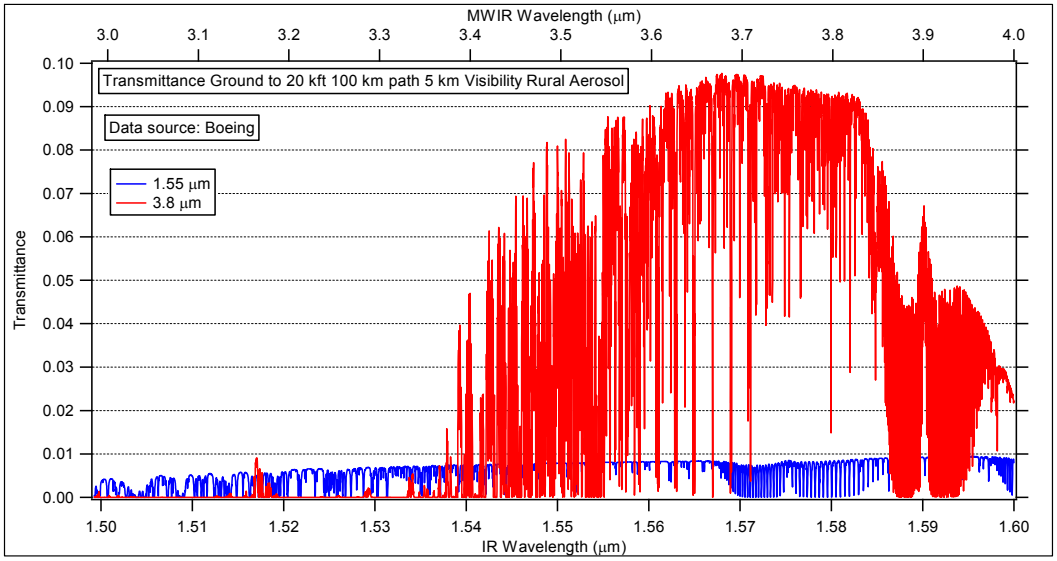

Fig. 1. Transmittance in the 1.5-1.6 μm band and the 3-4 μm band over 100 km path with elevation from ground to 20 kft with a 5 km visibility rural aerosol. Source: Boeing.

We report here on the free-space transmission of a homodyne return-to-zero quadrature phase-shift-keyed (RZ-QPSK) signal at 3.8 μm through a turbulent channel. A pair of Ti:PPLN-based integrated nonlinear wavelength converters developed by the Univ. of Paderborn was used to down-convert 1.55 to 3.8 μm at the transmitter and up-convert the transmitted 3.8 μm beam back to 1.55 μm for homodyne detection and demodulation. The experiment was conducted at a Boeing facility where the wind tunnel turbulence generator provided a weak turbulence transmission path. Test results show evidence that for a scintillation index value less than one (weak turbulence) 3.8 μm transmission is more robust than 1.55 μm. This is consistent with the weak turbulence theory where the scintillation index is approximately equal to the Rytov variance with a $\lambda^{-7/6}$ dependence. Extrapolated scintillation indexes for 3.8 and 1.55 μm using the Rytov variance and independent measurements at 632.8 nm are consistent with the RZ-QPSK scintillation data measured for 3.8 and 1.55 μm. Under the most severe turbulence condition, the average bit-error-rate (BER) of the 3.8 μm transmission is better than that of 1.55 μm, giving an estimated receiver sensitivity improvement of at least 6 dB. The RZ-QPSK signal, which has 2 bits per symbol, was operated at 80 MSym/s with a total data rate of 160 Mbits/s. The symbol rate in this case was limited by the transmitter and receiver board electronics. Turbulence-free transmission of a 3.8 μm QPSK signal at 2.488 Gbits/s using the same nonlinear converter pair has been demonstrated[4]. An atmospheric absorption test was not considered here due to the short transmission path length (< 5m) and the limited tuning range of our 1.55-μm laser source.

2. TRANSMISSION EXPERIMENT

A schematic of the transmission experiment is shown in Fig. 2. A 1.55 μm RZ-QPSK optical signal at 80 MSym/s is converted to 3.8 μm using a PPLN-based nonlinear converter[5]. The 3.8 μm optical beam was collimated and launched into a table-top wind tunnel[6] provided by Boeing. The 3.8 μm beam transmitted through the wind tunnel was collected and directed to a second nonlinear converter that up-converted the signal back to 1.55 μm. Fig. 3 shows a schematic of the nonlinear converter pair; both the down- and up-converters are pumped by the same 1100-nm source. The conversion efficiencies of the down- and up-converter are ~ 69 and 203 $\%W^{-1}$, respectively. Further details of the converter pair can be found in Ref. [5]. After up-conversion, the fiber-coupled 1.55 μm signal is directed to a RZ-QPSK receiver for homodyne detection. The RZ-QPSK transmitter and receiver are shown in Fig. 4 and Fig. 5.

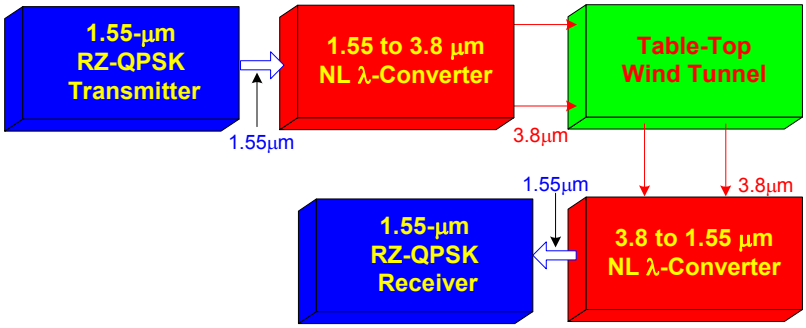

Fig. 2. Wind tunnel transmission test setup with nonlinear converter pair (1.55 to 3.8 µm and back to 1.55 µm).

The 1.55-µm RZ-QPSK transmitter consists of a narrow-linewidth laser (Laser 1) that operates near 1546.9 nm connected to a $LiNbO_3$ optical quadrature modulator[7] driven by a pair of 80 Mb/s bipolar RZ electrical data signals: I and Q. A custom-built electronic, FPGA-based, Tx board[8] provides the programmable bipolar RZ signals, pseudo-random binary sequence (PRBS) of a word length of 2^{14}-1 for the I and Q channels where Q was delayed from I by 8192 bits. The RZ-QPSK receiver subsystem receives and processes the optical QPSK signal as shown in Fig. 5 via a $LiNbO_3$ optical 90° hybrid[9] that combines the QPSK signal with the local laser (Laser 2) before balanced detection. The homodyne detected optical RZ-QPSK produces a pair of electrical signals: I and Q, at the outputs of the two sets of balanced photoreceivers as shown in Fig. 5. These signals are simultaneously captured by a pair of high-speed two-channel digitizers, sampling at 80 MS/s (1 sample per symbol). Up to 100M samples were captured or a 1.25s long of data stream. The digitizers were synchronized with the clock on the Tx board. The captured data were stored in a desktop computer for off-line processing using Matlab. Algorithms were applied to the captured data to recover the QPSK constellation so that the BER and the signal-to-noise ratio (SNR) of the received signal could be computed[10]. The minimum measurable BER per capture is about 10^{-8}. The received power is defined as the optical power of the 1.55 µm signal at the input of the RZ-QPSK receiver (after up-conversion) without turbulence. The transmission performance of 3.8 µm was compared with the 1.55 µm transmission through the wind tunnel with the converter pair bypassed.

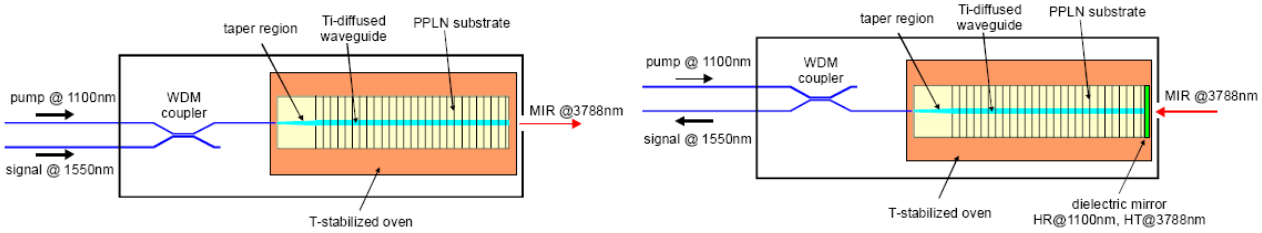

Fig. 3. Schematic of the PPLN-based Tx (left) and Rx (right) nonlinear wavelength converter pair.

Fig. 6 shows a photograph of the Boeing wind tunnel setup, the Tabletop Turbulence Generator (TTG). The TTG is composed of a small wind tunnel (4 inch test section) with a set of ¼ inch heated rods at the head of the test section. As indicated by the red arrow in the photograph, the 3.8 µm optical beam propagates into and out of the wind tunnel through a pair of CaF_2 windows attached to the sides of the wind tunnel. Turbulence generated by the wind tunnel is characterized by the air flow velocity and the temperature of the heated rods[6]. The index of refraction differences generate a complex phase field that can severely challenge high speed Laser Communication links. The character of the turbulence most closely resembles a boundary layer, since it is confined to a 4 inch layer, yet provides a substantial Optical Path Length (OPD) disturbance, up to ~ 0.1 microns. The approach is to generate a relatively uncontrolled, but well documented turbulent field. The turbulence is characterized by the scintillation index, measured from an image of a light mask and a Malley probe, measuring the angular fluctuations of the light transmitted through the wind tunnel. A series of test conditions (see Table 2) were used to cover a range of turbulence intensities and a range of temporal characteristics. The turbulent intensity was largely controlled by the temperature of the heated rods, which ranged from 400 – 900 degrees F. The temporal character of the turbulence was controlled by the flow velocity. This varied from 7.5 to 20 meters/second with correlation times varying from 0.6 to 0.85 milliseconds (measured to the ½ height of the

autocorrelation function). These correlation times correspond to eddy sizes of ~1.5 to 2 rod diameters (9.525 to 12.7 mm).

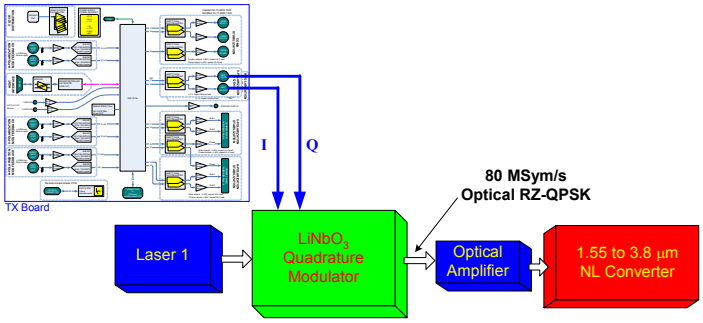

Fig. 4. RZ-QPSK optical transmitter setup with a nonlinear down-converter (1.55 to 3.8 μm).

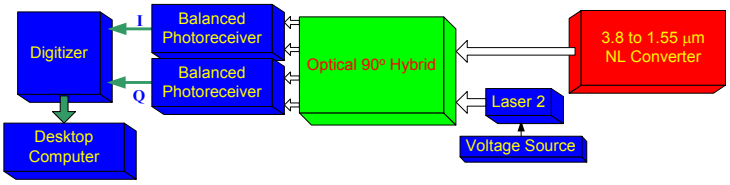

Fig. 5. RZ-QPSK receiver setup with a nonlinear up-converter (3.8 to 1.55 μm).

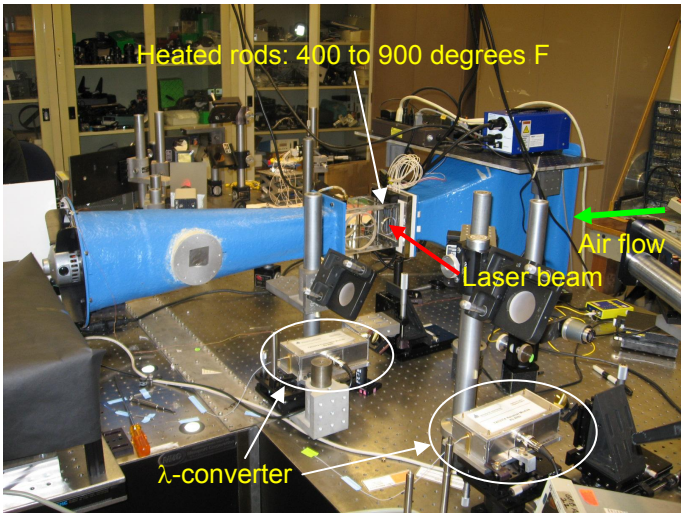

Fig. 6. Wind tunnel transmission test setup with nonlinear wavelength converter pair. Red arrow indicates the laser beam passes through the side window of the wind tunnel.

The receiver optic used for coupling the 3.8 μm beam into the PPLN waveguide is a 60° off-axis 1" diameter concave paraboloid with a 2" focal length. The f# is 2, which corresponds to a numerical aperture (NA) of 0.25. Table 1 shows NA of the PPLN waveguide computed for the 3.8 and 1.55 μm beams. Fig. 7 shows the calculated waveguide mode profiles at 3.8 and 1.55 μm. Due to the non-Gaussian beam shape in the waveguide the table shows NA value in the horizontal direction (h) and two NA values in the vertical direction (±v). Propagating a 3.8 μm beam with these numerical apertures, we underfill the optic with a beam that is roughly 0.44 × 0.76 inches. For transmission test of 1.55-μm through the wind tunnel the nonlinear converter pair was bypassed. In this case, the receiver optic used for coupling the 1.55 μm beam into a single-mode fiber is a 90 degree off-axis 1 inch diameter concave paraboloid with a

4-inch focal length. The f# is 4 giving a NA of 0.125. The NA for the coupling single-mode fiber is 0.067 and the beam diameter at the mirror is 0.54 inches.

Table 1. Computed NA of PPLN waveguide in the horizontal direction (h) and two NA values in the vertical direction (±v) for 3.8 and 1.55 μm beams.

	NA (h)	NA (+v)	NA (-v)
3.8 μm	0.11	0.25	0.13
1.55 μm	0.09	0.18	0.12

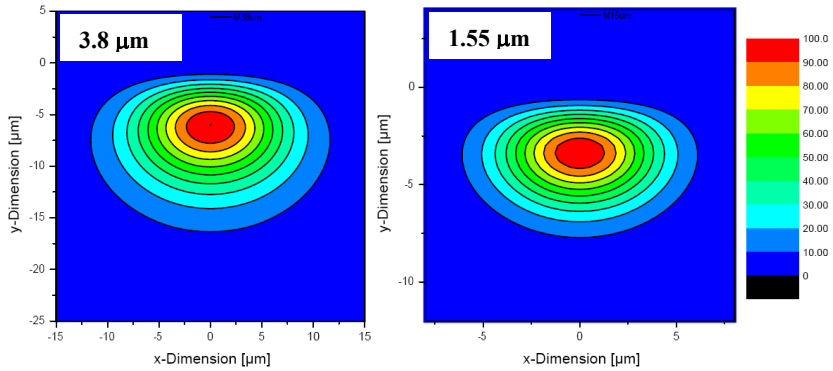

Fig. 7. Computed waveguide mode profiles for 3.8 μm (left) and 1.55 μm (right). Note the different scales of the two plots.

3. TRANSMISSION TEST RESULTS

Table 2 shows BER and SNR results of the received signal for 3.8 and 1.55 μm propagation through the wind tunnel for different air-flow velocities and temperatures. The no-turbulence received powers for 3.8 and 1.55 μm propagation are set to -39.5 and -33.5 dBm, respectively. It was observed that 3.8 μm propagation is much more robust to the turbulent environment in the wind tunnel than 1.55 μm. Because of this the received power was reduced significantly for the 3.8 μm case (-39.5 dBm) in order to obtain measurable BER (>10^{-8}) per 100M samples acquisition. As a comparison, Table **3** shows BER and SNR results for 3.8 μm propagating through the wind tunnel at a higher received power of -34 dBm. The transmission is virtually error-free in this case. Fig. 8 shows BER and SNR values from Table 2 versus the wind tunnel settings. Fig. 9 show plots of the received power fluctuation in time for 3.8 and 1.55 μm propagation through wind tunnel (V: 7.5m/s, T: 900F) computed from the captured I and Q signals. Also shown in the figure are histograms, autocorrelation traces, and spectra of the received power for the two wavelengths. It is clear that 3.8 μm suffers significantly less scintillation. An exponential fit of the received power autocorrelation trace gives a turbulence correlation time of about 0.5 ms. This is consistent with the expected 0.6 ms correlation time described earlier. Note the power fluctuation in the 3.8 μm transmission case without turbulence (black line of the top right plot in Fig. 9). This fluctuation has a prominent spectral peak at 60 and 120 Hz as can be seen in the bottom right plot shown in black in Fig. 9. This is likely a result of power line coupling into the electronics of the converter setup, e.g., pump laser electronics and the PPLN temperature controller. Slower power fluctuations (< 10 Hz) can be attributed to thermal fluctuations in the PPLN devices and mechanical vibrations.

From Table 2, the receiver sensitivity improvement using 3.8 μm relative to 1.55 μm is 6.9 dB (= -33.5 + 39.5 + 8.1583 - 7.2628) at the highest turbulence level setting of the wind tunnel (V: 7.5m/s, T: 900F). Note from Table 2 that in the case of no turbulence the total scintillation index for 3.8 μm is higher than that for 1.55 μm. This is attributed to non-turbulent related power fluctuation such as power line coupling to the converter setup described earlier. Because of this "intrinsic" non-turbulent related power fluctuation (in contrast to the "extrinsic" one caused by the wind tunnel) it is likely that the BER shown in Table 2 for 3.8 μm propagation will be lower if such "intrinsic" power fluctuations are

absent. This might also account for the discrepancies of BER at other wind tunnel parameters shown in Table 2 for 3.8 and 1.55 μm propagation.

Table 2. BER and SNR results for different wind tunnel parameters. Top panel: 3.8-μm propagation through wind tunnel. Bottom panel: 1.55-μm propagation through wind tunnel.

3.8-μm Propagation through Wind Tunnel

Wind Tunnel Parameters		Total Scintillation Index	Turbulence-Induced Scintillation Index	Received Power (dBm)	BER of I	BER of Q	SNR of I (dB)	SNR of Q (dB)
Velocity (m/s)	Temperature (F)							
No Turbulence	No Turbulence	0.21428	0	-39.5	1.30E-03	1.84E-03	9.5755	9.2603
10	400	0.22808	0.0138	-39.5	2.64E-03	1.87E-03	8.9101	9.2483
10	600	0.24407	0.02979	-39.5	3.76E-03	3.11E-03	8.5406	8.7428
10	800	0.29971	0.08543	-39.5	9.92E-03	9.74E-03	7.3451	7.3699
10	854	0.29449	0.08021	-39.5	8.10E-03	8.30E-03	7.6195	7.5874
15	400	0.23395	0.01967	-39.5	2.65E-03	2.87E-03	8.9075	8.8259
15	686	0.28086	0.06658	-39.5	7.36E-03	6.43E-03	7.7457	7.915
20	614	0.25603	0.04175	-39.5	4.80E-03	3.55E-03	8.2649	8.6028
7.5	**900**	**0.26426**	**0.04998**	**-39.5**	**5.26E-03**	**4.62E-03**	**8.1583**	**8.3101**

1.55-μm Propagation through Wind Tunnel

Wind Tunnel Parameters		Total Scintillation Index	Turbulence-Induced Scintillation Index	Received Power (dBm)	BER of I	BER of Q	SNR of I (dB)	SNR of Q (dB)
Velocity (m/s)	Temperature (F)							
No Turbulence	No Turbulence	0.10301	0	-33.5	1.01E-08	0.00E+00	14.9795	>14.984
10	400	0.22365	0.12064	-33.5	6.57E-07	6.75E-06	13.6926	12.7733
10	600	0.22016	0.11715	-33.5	9.19E-05	9.69E-05	11.4584	11.4274
10	800	0.32289	0.21988	-33.5	4.43E-03	4.46E-03	8.3572	8.3486
10	848	0.30785	0.20484	-33.5	6.61E-03	6.57E-03	7.8816	7.8888
15	400	0.21143	0.10842	-33.5	1.13E-04	1.63E-04	11.3342	11.1093
15	679	0.21033	0.10732	-33.5	6.96E-04	7.26E-04	10.0927	10.0602
20	603	0.21204	0.10903	-33.5	2.60E-04	2.40E-04	10.8061	10.8607
7.5	**900**	**0.63557**	**0.53256**	**-33.5**	**1.05E-02**	**1.05E-02**	**7.2628**	**7.2673**

Table 3. BER and SNR results for 3.8-μm propagation through wind tunnel for a received power of -34 dBm.

3.8-μm Propagation through Wind Tunnel

Wind Tunnel Parameters		Total Scintillation Index	Received Power (dBm)	BER of I	BER of Q	SNR of I (dB)	SNR of Q (dB)
Velocity (m/s)	Temperature (F)						
No Turbulence	No Turbulence	0.070639	-34	0	0	>14.984	>14.984
10	400	0.061519	-34	0	0	>14.984	>14.984
10	600	0.066677	-34	0	0	>14.984	>14.984
10	800	0.073372	-34	0	0	>14.984	>14.984
10	900	0.078747	-34	0	0	>14.984	>14.984
15	400	0.063704	-34	0	0	>14.984	>14.984
15	690	0.070246	-34	0	0	>14.984	>14.984
20	620	0.069789	-34	0	0	>14.984	>14.984
7.5	900	0.094825	-34	1.00E-08	0	14.9823	>14.984

A factor that contributes to the non-turbulence-induced BER is the laser frequency mismatch (> 1MHz) between the transmitter and the LO as a result of random frequency fluctuation of the lasers. For frequency mismatch less than 1 MHz, the QPSK signal can be recovered reliably using the phase rotation compensation algorithm[10]. However, there are instances in which the frequency mismatch is higher than 1 MHz due to the statistical nature of the laser frequency fluctuation. It is likely that the algorithm failed to recover the QPSK constellation for such instances. Bit errors not related to the turbulence are produced as a result. This also accounts for the discrepancies of BER shown in Table 2 for 3.8 and 1.55 μm propagation. The limitation of the algorithm to about 1 MHz frequency mismatch is due to the relatively low symbol rate. Higher symbol rates increase the laser frequency mismatch that can be compensated for by the algorithm.

The strength of the turbulence generated in the wind tunnel has been characterized independently at 632.8 nm. The scintillation index at 632.8 nm was recorded concurrently with the measurements for 1.55 and 3.8 μm transmission, wind tunnel parameters shown in Table 2. Table 4 and Table 5 show the scintillation index (S.I.) of the 632.8 nm optical beam measured using a Shack-Hartmann sensor[6] versus the wind tunnel setting. The S.I. is obtained from the variance of the spatial optical power across 200 spots, each 0.5 mm diameter and 1.5 mm separation, on the Shack-Hartmann image sensor.

The S.I. or the normalized intensity variance σ_I^2 for the received QPSK signal at 1.55 μm was calculated from samples of the captured I and Q signals, I_k and Q_k. A total of 100M samples were captured (1.25 sec) per acquisition at a sampling rate of 80MS/s. For homodyne detection, the received signal optical power is proportional to $I_k^2 + Q_k^2$. An instantaneous optical power for the *k*th sample was computed using $P_k = I_k^2 + Q_k^2$, where $k = 1, 2, ...100\text{M}$. The S.I. was computed based on values of P_k for all 100M samples using $\left[\left\langle P_k^2 \right\rangle / \left\langle P_k \right\rangle^2\right] - 1$.

Under the weak turbulence condition with $\sigma_I^2 < 1$, the normalized intensity variance is approximately equal to the Rytov variance σ_R^2 for plane wave as follows

$$\sigma_I^2 = \left[\left\langle I^2 \right\rangle / \left\langle I \right\rangle^2\right] - 1 \approx \sigma_R^2 = 1.23 C_n^2 \left(2\pi/\lambda\right)^{7/6} L^{11/6},$$

where I is the received intensity, λ is the optical wavelength, C_n^2 is the refractive index structure parameter (assumed independent of λ), and L is the propagation distance. Therefore, under the same turbulence and propagation conditions the S.I. at a wavelength λ can be deduced from another wavelength λ_0 at which the S.I. is known via the relation

$$\sigma_I^2(\lambda) \approx 1.23 C_n^2 \left(2\pi/\lambda\right)^{7/6} L^{11/6} = \sigma_I^2(\lambda_0)\left(\lambda_0/\lambda\right)^{7/6}.$$

The S.I. at 3.8 μm can be deduced from the 632.8-nm measurement as follow

$$\sigma_{I-3.8\mu\text{m}}^2 \approx \sigma_I^2(632.8\,\text{nm})\left(\frac{632.8}{3807.54}\right)^{7/6} = \frac{\sigma_I^2(632.8\,\text{nm})}{8.1147}, \text{ Eqn. (1)}$$

and for 1.55 μm

$$\sigma_{I-1.55\mu\text{m}}^2 \approx \sigma_I^2(632.8\,\text{nm})\left(\frac{632.8}{1546.9}\right)^{7/6} = \frac{\sigma_I^2(632.8\,\text{nm})}{2.8372}, \text{ Eqn. (2)}$$

Using the above relations, the turbulence-induced S.I. at 3.8 and 1.55 μm extrapolated from Eqns. (1) and (2) are tabulated in Table 4 and Table 5 along with the measured S.I. at 632.8 nm, $\sigma_I^2(632.8\,\text{nm})$. The turbulence-induced S.I. is simply the total S.I. minus the no-turbulence scintillation index. Turbulence-induced S.I. measured at 3.8 and 1.55 μm shown in Table 2 are also listed in Table 4 and Table 5 for comparison. The turbulence-induced S.I. values shown in Table 4 and Table 5 versus the wind tunnel setting are plotted in Fig. 10. One can see readily see that the measured S.I. for 1.55 and 3.8 μm matches quite well within experimental uncertainties with the extrapolated S.I. deduced from the 632.8 nm S.I. This shows that the 1.55 and 3.8 μm transmission measurements are consistent with the weak turbulence theory.

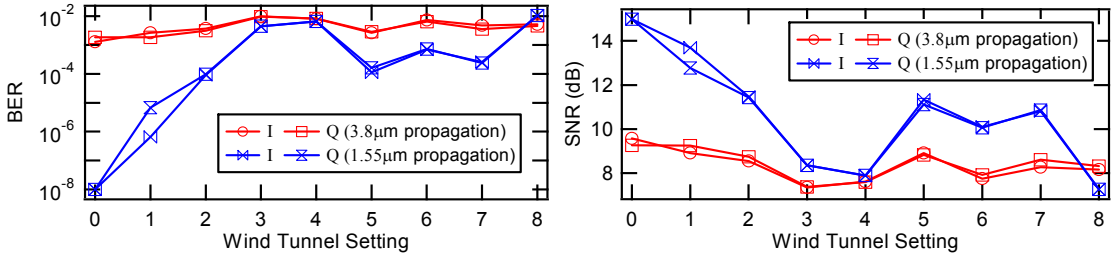

Fig. 8. BER (left) and SNR (right) values in Table 2 versus wind tunnel setting. Setting 0 to 8 corresponds to rows 1 (no turbulence) to 9 (V: 7.5m/s, T: 900F) for the wind tunnel parameters column in the table.

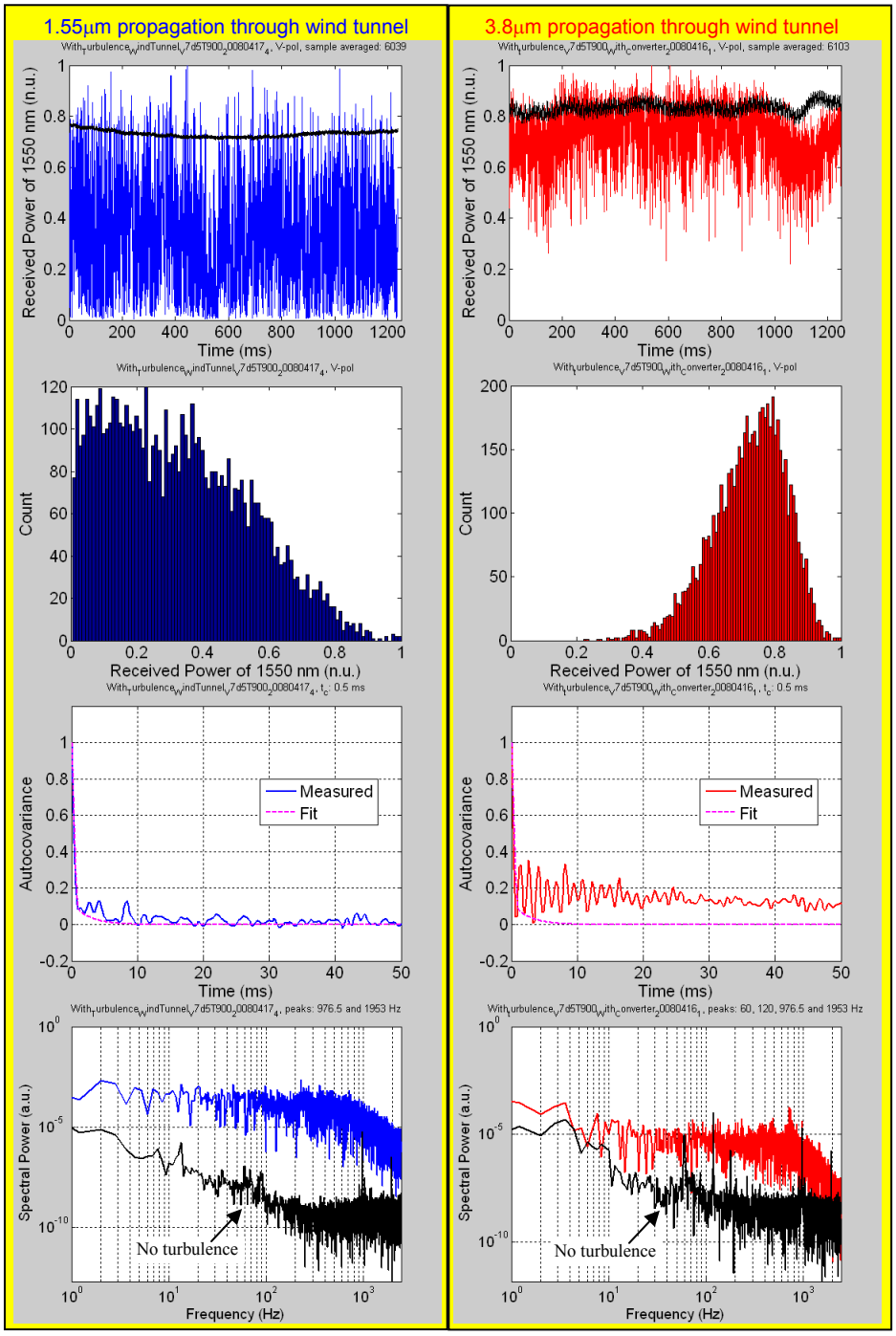

Fig. 9. Top to bottom row: received power versus time, histogram of the received power, autocorrelation of the received power, and spectra of the received power. Left and right columns are 1.55 and 3.8 μm propagation through wind tunnel at V: 7.5m/s and T: 900F, respectively. Black lines in the plots on the top row are received power with no turbulence. Lower black curves in the bottom row plots are received power spectra without turbulence. Scintillation indexes for 1.55 and 3.8 μm are 0.53 and 0.05, respectively.

Table 4. Turbulence-induced scintillation index measured at 632.8 nm and at 3.8 μm for different wind tunnel parameters. The S.I. at 3.8 μm from Eqn. (1) is also shown.

632.8-nm/3.8-μm Propagation through Wind Tunnel					
Wind Tunnel Setting	Wind Tunnel Parameters		Turbulence-Induced Scintillation Index (S.I.)		
	Velocity (m/s)	Temperature (F)	S.I. at 632.8 nm (Measured by Boeing)	S.I. at 3.8 μm from Eqn. (1)	Measured S.I. at 3.8 μm
			$\sigma_I^2(632.8\text{nm})$	$\sigma_{I\text{-}3.8\,\mu\text{m}}^2$	$\sigma_I^2(3.8\mu\text{m})$
1	10	400	0.362	0.0446102	0.0138
2	10	600	0.413	0.0508951	0.02979
3	10	800	0.57	0.0702426	0.08543
4	10	854	0.633	0.0780062	0.08021
5	15	400	0.246	0.0303152	0.01967
6	15	686	0.378	0.0465819	0.06658
7	20	614	0.31	0.0382021	0.04175
8	7.5	900	0.729	0.0898366	0.04998

Table 5. Turbulence-induced scintillation index measured at 632.8 nm and at 1.55 μm for different wind tunnel parameters. The S.I. at 1.55 μm from Eqn. (2) is also shown.

632.8-nm/1.55-μm Propagation through Wind Tunnel					
Wind Tunnel Setting	Wind Tunnel Parameters		Turbulence-Induced Scintillation Index		
	Velocity (m/s)	Temperature (F)	S.I. at 632.8 nm (Measured by Boeing)	S.I. at 1.55 μm from Eqn. (2)	Measured S.I. at 1.55 μm
			$\sigma_I^2(632.8\text{nm})$	$\sigma_{I\text{-}1.55\,\mu\text{m}}^2$	$\sigma_I^2(1.55\mu\text{m})$
1	10	400	0.35	0.12336	0.12064
2	10	600	0.503	0.177285	0.11715
3	10	800	0.613	0.216056	0.21988
4	10	848	0.656	0.231211	0.20484
5	15	400	0.444	0.15649	0.10842
6	15	679	0.421	0.148384	0.10732
7	20	603	0.371	0.130761	0.10903
8	7.5	900	0.696	0.245309	0.53256

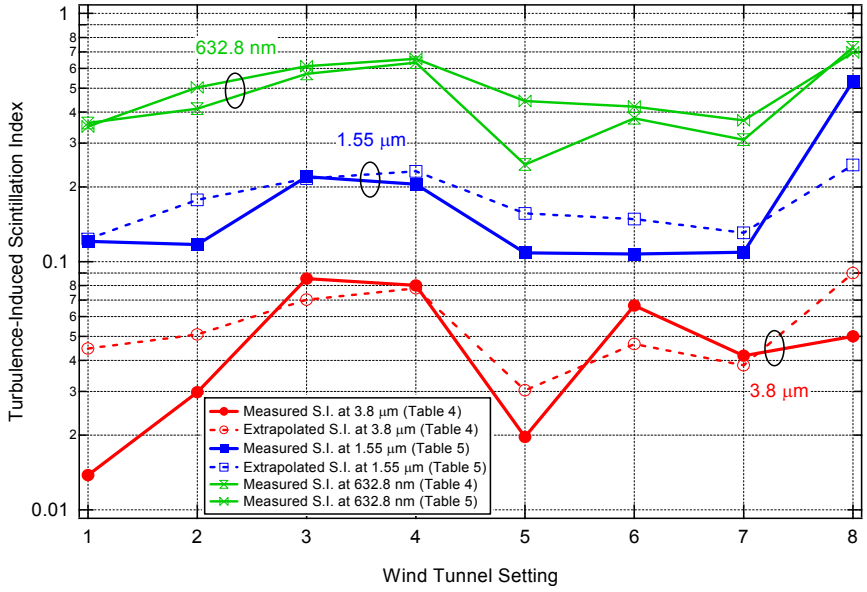

Fig. 10. Turbulence-induced scintillation index from Table 4 and Table 5 plotted in logarithmic scale versus wind tunnel setting.

4. CONCLUSIONS

In summary, comparison of transmission between 1.55 and 3.8 μm through wind tunnel reveals the following: under weak turbulence 3.8 μm transmission is more robust than 1.55 μm. This is consistent with the wavelength dependence of the Rytov variance, which is approximately equal to the scintillation index for the case of weak turbulence. Under the same turbulence condition, the turbulence-induced scintillation index measured at 3.8 μm is consistently lower than that at 1.55 μm. Wind tunnel test results for 3.8 and 1.55 μm are consistent with weak turbulence theory where the scintillation index varies as $\lambda^{-7/6}$. Extrapolated scintillation indexes using the Rytov variance for 3.8 and 1.55 μm based on measured data at 632.8 nm are consistent with scintillation indexes obtained from the RZ-QPSK transmission data for 3.8 and 1.55 μm. Under the most severe turbulence condition, the average BER of 3.8 μm is better than 1.55 μm giving an estimated receiver sensitivity improvement of at least 6 dB.

Transmission test for 3.8 μm under strong turbulence was not conducted since our strong-turbulence generator, phase plates, is not operable at wavelengths other than 1.55 μm[10]. Nevertheless, transmission performance of 3.8 μm under strong turbulence is expected to be comparable or worse than 1.55 μm depending on C_n^2 and the range. This has been analyzed theoretically by Boeing and is summarized in the Appendix.

APPENDIX: SCINTILLATION VERSUS WAVELENGTH

The data collected during these tests was used to extract a scintillation index. Those results exhibited a rather strong wavelength dependence, calculated from the communications signal. The TTG uses instrumentation at ~0.6 microns, while the communications wavelengths through the TTG were at 1.55 microns and 3.8 microns. The turbulence states generated by the TTG fall into the class of WEAK TURBULENCE.

The question naturally arises, what should the difference in scintillation index be for those two wavelengths for practical conditions, including STRONG TURBULENCE? Recent literature has addressed these issues with analytical expressions for the scintillation index in various conditions (Andrews et al.). Below we show the results of calculations of the expected performance following the methods and results published in "Laser Beam Scintillation with Applications", SPIE, 2001, Andrews, Phillips, Hopen.

Andrews et al executed first principle analyses of scalar electromagnetic field propagation using an Extended Huygens-Fresnel Principle, which is expected to be superior to the classical Rytov Approximation for strong turbulence. Both methods limit the analysis to first and second order perturbations. The statistical variances of the received fields are constructed for three canonical propagating fields: plane wave, spherical wave, and Gaussian beam. Due to time limitations, we restrict this analysis to the spherical wave models.

The scintillation index is routinely defined using the 4-th order moments of the field as the variance of the Irradiance at a single point in the pupil plane:

$$\sigma_I^2(\vec{r},L)=\frac{\left\langle I^2(\vec{r},L)\right\rangle}{\langle I(\vec{r},L)\rangle^2}-1,$$

where I is the irradiance field as a function of the distance from the receiver, L, and $\vec{r}$ is the distance off of the beam axis. In the Rytov Approximation, this variance is given as $\sigma_{IR}^2=1.23C_n^2k^{7/6}L^{11/6}$. Again this is generally valid for Weak Turbulence, but it is used as a turbulence strength parameter helping identify regions of strong turbulence. Here k is the optical wavenumber, L is the distance from the transmitter to the receiver, and C_n^2 is the index of refraction structure parameter of the atmosphere.

For a spherical wave in arbitrary turbulence, the following expression is obtained:

$$\sigma_I^2(L) = Exp\left(\frac{0.21 \cdot \sigma_{IR}^2}{\left(1+0.56 \cdot \sigma_{IR}^{12/5}\right)^{7/6}} + \frac{0.20 \cdot \sigma_{IR}^2}{\left(1+0.69 \cdot \sigma_{IR}^{12/5}\right)^{5/6}} \right).$$

Below we have plotted the scintillation index (Vertical Scale) as a function of range (m) for three wavelengths: 0.5 microns (Blue), 1.55 microns (Green), and 3.8 microns (Red), for C_n^2 = 5.0x10^{-13} m$^{-2/3}$, which is a moderate level of turbulence.

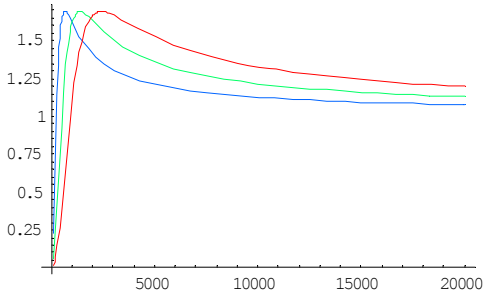

Note that for ranges out to ~ 1 kilometer, the theory predicts 3.8 microns (MWIR) scintillation to be much less than scintillation at 1.55 microns. This is consistent with our experimental results.

We also note that for longer ranges, the large advantage at 3.8 microns becomes a modest disadvantage. That is, beyond ~2 kilometers, they cross over, and the scintillation at 3.8 microns is slightly higher than at 1.55 microns.

Finally, this exhibits a feature that is common for strong turbulence, the scintillation peaks, and then saturates at a fairly constant level for long propagation distances.

For weak turbulence, C_n^2 = 5.0x10^{-14} m$^{-2/3}$, and the crossover still exists, but it now occurs beyond 5 km, as seen in the following plot. After the crossover, MWIR suffers 10-15% more scintillation. Also the turbulence saturates at longer ranges as well.

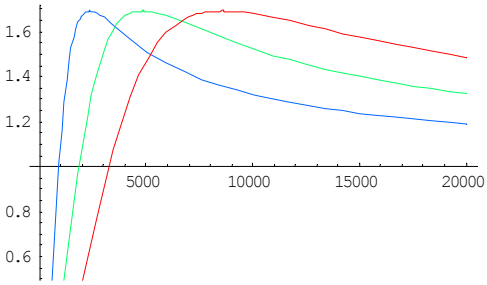

Next we plot the case of strong turbulence, C_n^2 = 5.0x10^{-12} m$^{-2/3}$, where we find saturation occurring at much shorter ranges, so the advantage exists for only a very short range, only a few hundred meters.

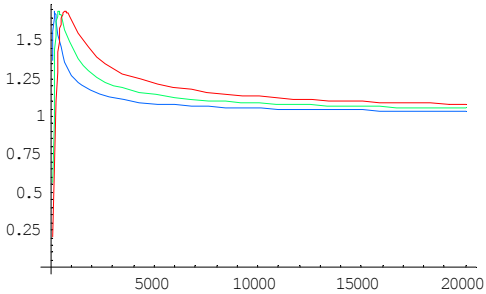

It is instructive to calculate the DIFFERENCE in the scintillation index at 1.55 microns and 3.8 microns. The next plot shows the difference (1.55 scintillation – 3.8 scintillation) for the three cases of weak (Green), moderate (Blue), and strong turbulence (Purple). Positive values mean scintillation is larger at 1.55 microns, negative values mean scintillation is smaller at 1.55 microns.

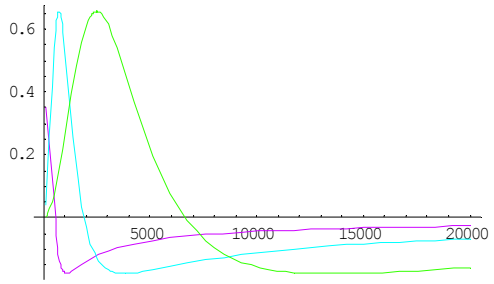

The theoretical model used in these calculations is too incomplete to represent the real case of Gaussian propagation, nor does it include inner and outer scale effects. More complete models show similar features for a fixed wavelength, and we expect similar trends versus wavelength.

ACKNOWLEGEMENTS

This research was supported by the DARPA TACOTA program. The authors thank C. Langrock for technical assistance.

REFERENCES

[1] Prasad, N., "Optical communications in the mid-wave IR spectral band," J. Opt. Fiber Commun. Rep., **2**, 558-602 (2005).

[2] Tabirian, A. M., Stanley, D. P., Roberts, D. E., and Thompson, A. B., "Atmospheric propagation of novel MWIR laser output for emerging free-space applications," Proc. of SPIE Vol. 6951, 69510T, (2008).

[3] Mahon, R., Burris, H. R., Ferraro, M.S., Moore, C.I., Rabinovich, W.S., Suite, M.R., Bewley, W. W., Canedy, C. L., Larrabee, D., Meyer, J. R., and Vurgaftman, I., "A comparative study of 3.6μm and 1.55μm atmospheric transmission," Proc. of SPIE Vol. 6951, 69510Q, (2008).

[4] Ip, E., Büchter, D., Langrock, C., Kahn, J. M., Herrmann, H., Sohler, W., and Fejer, M. M., "QPSK transmission over free-space link at 3.8 μm using coherent detection with wavelength conversion," ECOC 2008, 21-25 September 2008, Brussels, Belgium, paper Tu.3.E7.

[5] Büchter, D., Herrmann, H., Langrock, C., Fejer, M., and Sohler, W., "Integrated optical PPLN transmitter and receiver modules for wavelength conversion of C-band signals to/from the mid infrared," ECOC 2008, 21-25 September 2008, Brussels, Belgium, paper P.2.24.

[6] Soreide, D., Saint Clair, J., Cassaday, P., "A tabletop turbulence generator," SPIE Defense Security Symposium, 17-20 March, 2008, Orlando, Florida, paper 6951-19.

[7] Cho, P. S., Khurgin, J., and Shpantzer, I., "Closed-loop bias control of optical quadrature modulator," IEEE Photonics Technology Letters, vol. 18, no. 21, pp. 2209-2211, November, 2006.

[8] Cho, P. S., Meiman, Y., Harston, G., Achiam, Y., and Shpantzer, I., "Fading mitigation in homodyne RZ-QPSK via delay-diversity transmission," Coherent Optical Technology and Application, Boston, Massachusetts, 13-16 July 2008, paper CWB6.

[9] Cho, P. S., Harston, G., Kerr, C., Greenblatt, A., Kaplan, A., Achiam, Y., and Shpantzer, I., "Coherent homodyne detection of BPSK signals using time-gated amplification and $LiNbO_3$ optical 90^o hybrid," IEEE Photonics Technology Letters, vol. 16, no. 7, pp. 1727-1729, July, 2004.

[10] Cho, P. S., Harston, G., Soreide, D., Saint Clair, J. M., Achiam, Y., and Shpantzer, I., "Mitigation of weak and strong turbulence-induced fading in optical homodyne RZ-QPSK via delay-diversity transmission," SPIE Defense, Security, and Sensing 2009, Orlando, Florida, paper 7324-22.